Ceramics International xxx (xxxx) xxx–xxx

Contents lists available at ScienceDirect

Ceramics International

journal homepage: www.elsevier.com/locate/ceramint

A novel $Ce_2Zr_3(MoO_4)_9$ microwave dielectric ceramic with ultra-low firing temperature

B.J. Tao, C.F. Xing, W.F. Wang, H.T. Wu*, Y.Y. Zhou**

School of Materials Science and Engineering, University of Jinan, Jinan, 250022, China

ARTICLE INFO

Keywords:
$Ce_2Zr_3(MoO_4)_9$
Chemical bonds theory of complex crystals
Low-temperature sintering
Far infrared reflectivity spectra

ABSTRACT

A new type of $Ce_2Zr_3(MoO_4)_9$ (CZM) ceramic was successfully prepared through the solid-phase reaction process at low sintering temperature. All the studied sintered samples exhibited a trigonal phase with space group of R-3c (No.167) by means of X-ray diffraction. Rietveld refinement analysis results further explored the crystalline structure of CZM. According to Scanning electron microscopy images, dense uniform surface morphology was observed at 525–625 °C for CZM ceramics. The correlations between structural characteristics and microwave dielectric properties of CZM ceramics were systematically investigated by calculating some chemical bond parameters on the basis of the chemical bonds theory of complex crystals. The analysis results of far-infrared reflectivity spectroscopy revealed that the absorption of structural phonon vibration at infrared frequencies played a dominant role in dielectric polarization contribution for CZM ceramics. Furthermore, the CZM sample sintered at 575 °C exhibited optimum microwave dielectric properties of $\varepsilon_r = 10.69$, $Qf = 19{,}062$ GHz and $\tau_f = -1.29$ ppm/°C.

1. Introduction

Because of the importance of integration and miniaturization for microwave circuit system, the low-temperature co-fired ceramics (LTCC) technology has been explored. Ceramics with high ε_r values, high Qf values, near-zero τ_f values and low sintering temperatures are widely tried to design the LTCC devices [1,2]. It is urgently to develop microwave dielectric ceramics with low sintering temperatures and excellent microwave dielectric properties to satisfy the rapid advancement in communication industry. Therefore, there is a strong drive to develop new microwave dielectric ceramics [3–8], lower temperatures by adding sintering additives [9–11] and improve microwave dielectric properties by ion substitution [12–15]. Especially, a series of new microwave dielectric ceramics, such as MoO_3, $[Ca_{0.55}(Sm_{1-x}Bi_x)_{0.3}]MoO_4$ and (Ca, Bi)(Mo, V)O_4 ceramics, have been studied in detail [16–18].

Recently, as shown in Table 1, Mo-based microwave dielectric ceramics, such as $Sm_2Zr_3(MoO_4)_9$, $Nd_2Zr_3(MoO_4)_9$ and $Eu_2Zr_3(MoO_4)_9$, etc., have achieved great attention owing to the excellent microwave dielectric properties and low sintering temperatures [19–22]. For example, $La_2Zr_3(MoO_4)_9$ ceramic sintered at 775 °C was reported with good microwave dielectric properties of $\varepsilon_r = 10.8$, $Qf = 50{,}628$ GHz and $\tau_f = -38.8$ ppm/°C [20]. However, a new $Ce_2Zr_3(MoO_4)_9$ ceramic have not been reported up to now. Therefore, the CZM samples were prepared successfully via the solid-state route for the first time. The microstructures, sintering characteristics and microwave dielectric properties of CZM were studied scientifically. The chemical bonds theory of complex crystals and infrared (IR) reflectivity spectra were helpful to explore the relationships between the intrinsic factors and dielectric properties of CZM samples.

2. Experimental procedure

The CZM samples were prepared by the standard solid-state reaction route. High purity raw materials of cerium oxide (CeO_2, 99.9%, Macklin), zirconium dioxide (ZrO_2, 99.99%, Macklin), and molybdenum trioxide (MoO_3, 99.95%, Nine-Dinn chemistry Shanghai Co., Ltd, China) were accurately weighed in CeO_2–ZrO_2–MoO_3 system with molar ratio 2:3:9. The mixed powders were placed in nylon pot with the spherical ZrO_2 ceramics and anhydrous alcohol as grinding medium, and then the ball-machine was set to rotate at 200 r/min for ball-milling for 24 h. The obtained slurries separated from zirconia spheres were dried in an open oven and then calcined at 700 °C for 2 h. The pre-sintered powders were re-grounded for 24 h, and dried at 80 °C once more. Afterwards, the granulated that added with 10 % PVA as an adhesive were pressed into cylinders sample under a uniaxial pressure of 200 MPa. At last, the prepared CZM disks were sintered at

* Corresponding author.
** Corresponding author.
E-mail address: mse_wuht@ujn.edu.cn (H.T. Wu).

https://doi.org/10.1016/j.ceramint.2019.08.206
Received 14 July 2019; Received in revised form 20 August 2019; Accepted 22 August 2019

Table 1
Summarized microwave dielectric properties of Mo-based microwave dielectric ceramics.

Materials	Sintering temperatures (°C)	ε_r	Qf (GHz)	τ_f (ppm/°C)	References
$Sm_2Zr_3(MoO_4)_9$	875	11.0	74,012	−45.3	[19]
$Nd_2Zr_3(MoO_4)_9$	850	10.8	58,942	−40.9	[19]
$La_2Zr_3(MoO_4)_9$	775	10.8	50,628	−38.8	[20]
$La_2Zr_3(MoO_4)_9$	650	10.8	61.790	−29.1	[21]
$La_2(Zr_{0.92}Ti_{0.08})_3(MoO_4)_9$	750	10.33	80,658	3.48	[21]
$Eu_2Zr_3(MoO_4)_9$	600	10.75	74,900	−8.88	[22]
$Ce_2Zr_3(MoO_4)_9$	575	10.69	19,062	−1.29	This work

500–625 °C for 4 h under air atmosphere.

The phase structures of the sintered CZM ceramics were characterized via an X-ray diffractometer (XRD: D8 Advance, Bruker Co., Germany) with nickel-filtered Cu-Kα radiation (λ = 1.542 Å, 40 kV/40 mA). The FullProf_Suite program [23] was employed to obtain the unit cell parameters from the Rietveld refinement of XRD data. The sintered specimens were magnified appropriate times to observe the surface micro-structures by using QUANTA 250FEG type Scanning electron microscope (SEM: FEI Co., United States) coupled with EDS. The room-temperature infrared reflectivity spectrum data of thin polished disc (around at 1 mm) were taken using a Fourier transform infrared spectrometer (FTIR: Bruker IFS 66v) at National Synchrotron Radiation Laboratory (NRSL, BL01B infrared beamline station, University of Science and Technology of China). The dielectric constants were measured at approximately 12.5–13.5 GHz in the light of Hakki-Coleman dielectric resonator method [24]. The unload quality factors were measured with the help of $TE_{01\delta}$ cavity method [25] using TE01d mode where a pellet was placed in metal shielded cavity to determine the coupling energy of the entire system through the coaxial probe. The temperature coefficient of resonant frequency values were attained by using Eq. (1):

$$\tau_f = \frac{f_T - f}{60 \times f_0} \times 10^6 (ppm/°C) \quad (1)$$

where, f_T and f_0 were the resonant frequency at 85 °C and 25 °C, respectively.

The apparent densities of as-fired samples were gauged through liquid Archimedean method (FR124 N electronic balance, Ohaus Instruments Shanghai Co., Ltd.) utilizing deionized water as liquid media. The theoretical densities (ρ_{theory}) were estimated by formula (2):

$$\rho_{theory} = \frac{ZA}{V_c N_A} (g/cm^3) \quad (2)$$

where V_c was volume of refined unit-cell (cm^3), N_A was Avogadro constant ($6.023 \times 10^{23}\ mol^{-1}$), Z was atomic unit cell number (Z = 6 in this study), A represented the relative atomic weight ($g \cdot mol^{-1}$). The following equation was applied to reckon the relative density ($\rho_{relative}$):

$$\rho_{relative} = \frac{\rho_{apparent}}{\rho_{theory}} \times 100\ \% \quad (3)$$

3. Results and discussion

Fig. 1 simultaneously presented the typical XRD patterns of CZM sample sintered at 500–625 °C for 4 h and the calcined powders sintered at 700 °C for 2 h. It could be seen that the XRD diffraction peak positions of all experimental specimens matched well with $Pr_2Zr_3(MoO_4)_9$-like crystal structure. And there were no traces of the additional impurity phases during the sintering process, which indicated that the pure single trigonal solid-solution phase structure with a R-3c (167) space group was formed in all samples.

In view of Rietveld refinement method (Fig. 2), the refined lattice parameters of the samples sintered within the temperature range of 500–625 °C from XRD data were gained so as to better investigate the

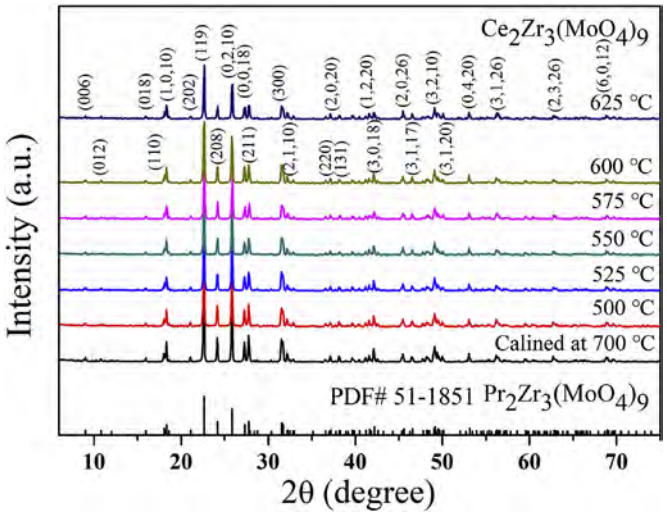

Fig. 1. XRD patterns of Ce2Zr3(MoO4)9 ceramics sintered at 500–625 °C.

CZM structure at great length, where $Nd_2Zr_3(MoO_4)_9$ (ICSD File No. 92,600) served as initial structural model. Fig. 3 depicted the variation tendencies of lattice parameters. The a and b gradually increased with the increasing sintering temperature, and c was roughly stable at 58.8629 Å, which resulted in the increase of V_m from 4929.10 $Å^3$ at 500 °C to 4932.40 $Å^3$ at 625 °C. The structural parameters and refined discrepancy factors (R_{wp}, R_p, and χ^2) after Rietveld refinement were all listed in Table 2. R_p, R_{wp} and χ^2 were measured as 7.08–8.73%, 9.20–11.0% and 1.57–2.09, respectively, which confirmed the phase purity of CZM.

The schematic illustration of trigonal structured CZM sample was shown in Fig. 4, and Table 3 exhibited the occupations and the refined atomic positions of CZM sample. The CZM crystal was constituted of CeO_9, ZrO_6 and MoO_4 polyhedra, which were shared by vertices. In this structure, Ce, Zr(1), Zr(2), Mo(1), Mo(2) and O atoms occupied the 12c, 6b, 12c, 36f,18e and 36f Wyckoff positions, respectively.

Fig. 5 illustrated the apparent and relative densities of CZM samples sintered at 500–625 °C. When the temperature increased to 575 °C, apparent density increased from 3.59 to the maximum value of 3.84 g/cm^3, and then reached a saturated value of 3.83 g/cm^3 at 575–625 °C. The increase in density was due to the decrease of porosity. Just like the trend of apparent density, the relative density increased from 88.99 % at 500 °C to 95.30 % at 575 °C and then kept stable. SEM micrographs sintered at 500–625 °C for 4 h were shown in Fig. 6. Slight pores were observed at a lower temperature of 500 °C, and dense microstructures with clear grain boundaries could be obtained as shown in Fig. 6(b)–(f). EDS of CZM sample sintered at 575 °C was shown in Fig. 6(g). Atom ratio of Ce, Zr, Mo and O were 2.85 %, 5.43 %, 15.00 % and 76.73 % respectively, which was consistent with chemical formula of CZM.

Microwave dielectric properties for CZM samples sintered at 500–625 °C were presented in Fig. 7. With temperature increasing, dielectric constant increased from 9.51 at 500 °C to 10.69 at 575 °C, and then saturated at 575–625 °C. It was obvious that the variation in

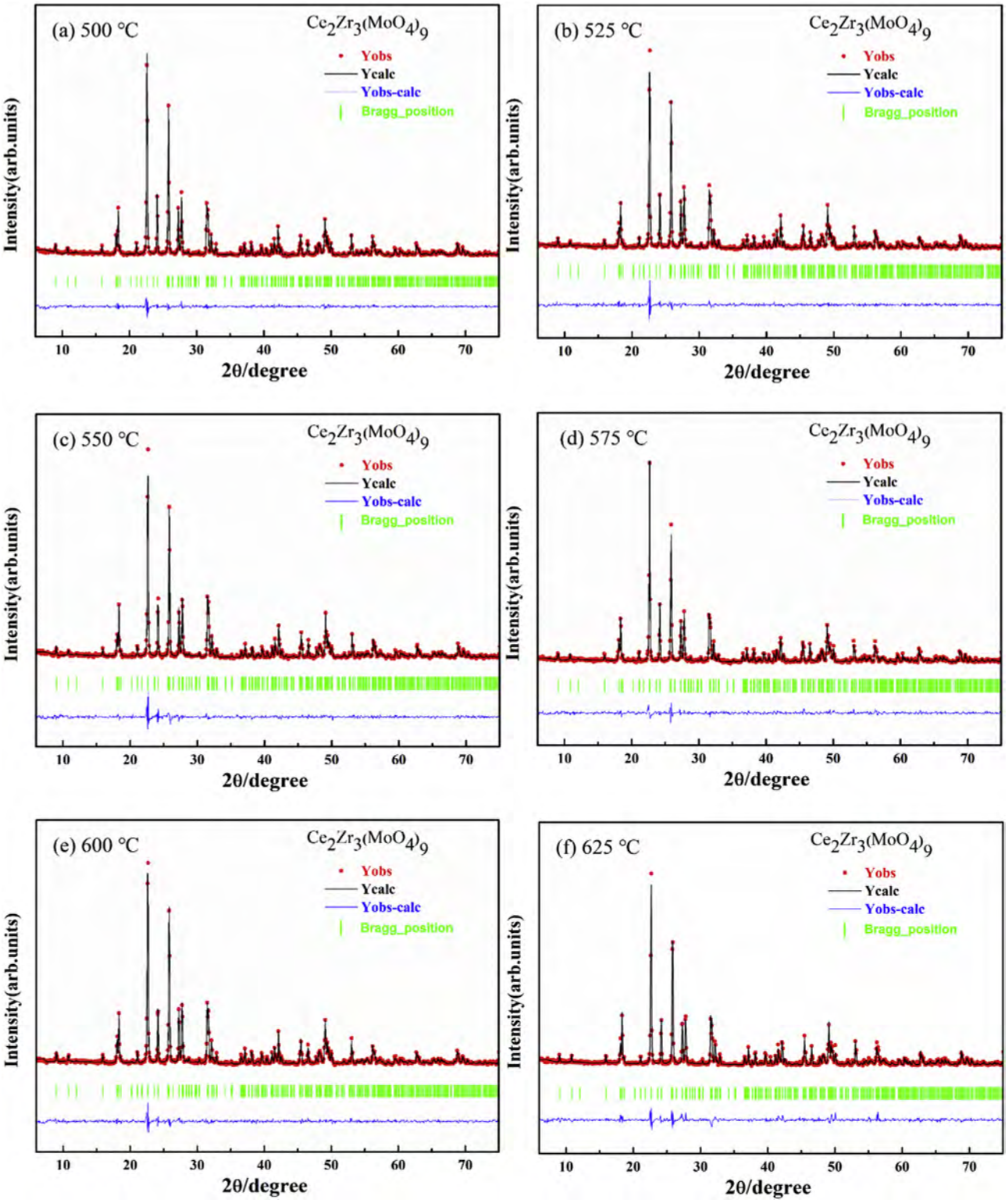

Fig. 2. Rietveld refinement of Ce2Zr3(MoO4)9 ceramics sintered at different temperatures (a-f corresponding to 500–625 °C).

dielectric constant was consistent with the density. The higher density corresponded to higher dielectric constant. The dielectric constant of ceramic with single phase is mostly related to the density and polarizability. To further investigate the effect of polarizability on dielectric constant, molecular polarizability of CZM sample is calculated according to Shannon's report based on Eq. (4) [26].

$$\alpha_{theo.} = 2\alpha(Ce_2Zr_3(MoO_4)_9) = 2\alpha((Ce^{3+}) + 3\alpha(Zr^{4+}) + 9\alpha(Mo^{6+}) + 36\alpha(O^{2-}) \quad (4)$$

where α of Ce^{3+}, Zr^{4+} and O^{2-} are the theoretical ion polarizabilities reported by Shannon et al. [26] and $\alpha(Mo^{6+})$ is calculated by Choi et al. [27]. The observed value dielectric polarizability is obtained by using Clausius-Mosotti equation (5):

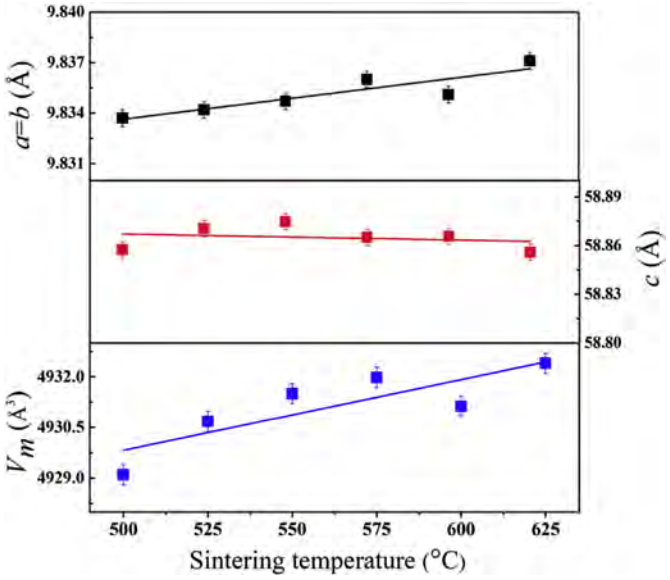

Fig. 3. The variation tendencies of lattice parameters with sintering temperature.

Table 2
The refinement parameters, theoretical densities and relative densities of $Ce_2Zr_3(MoO_4)_9$ ceramics fired at 500–625 °C.

Structural parameters	sintering temperature (°C)					
	500	525	550	575	600	625
$a = b$ (Å)	9.8337	9.8342	9.8347	9.8360	9.8351	9.8371
c (Å)	58.8574	58.8705	58.8747	58.8650	58.8656	58.8559
$\alpha = \beta$ (°)	90	90	90	90	90	90
γ (°)	120	120	120	120	120	120
V_m (Å^3)	4929.10	4930.68	4931.50	4931.98	4931.13	4932.40
R_p (%)	7.08	7.26	7.53	7.53	7.30	8.73
R_{wp} (%)	9.20	9.33	9.76	9.86	9.38	11.0
χ^2	1.61	1.57	1.68	1.67	1.66	2.09
$\rho_{theo.}$ (g·cm^{-3})	4.0305	4.0293	4.0286	4.0282	4.0289	4.0279
$\rho_{rela.}$ (%)	88.99	92.28	94.14	95.30	95.07	94.96

$\rho_{thep.}$— theoretical density of $Ce_2Zr_3(MoO_4)_9$ ceramics.
$P_{rela.}$— relative density of $Ce_2Zr_3(MoO_4)_9$ ceramics.
R_p — reliability factor of patterns.
R_{wp} — the reliability factor of weighted patterns.
χ^2 — goodness of fit indicator = chi^2 = $(R_{wp}/R_{exp})^2$.

Table 3
Atomic fractional coordinates of the $Ce_2Zr_3(MoO_4)_9$ ceramics fired at 575 °C.

Atom	Wyckoff position	Site	x	y	z	Occupancy
Ce	12c	3	0.6667	0.3333	0.0297	0.3333
Zr1	6b	−3	0.0000	0.0000	0.0000	0.1667
Zr2	12c	3	0.3333	0.6667	0.0707	0.3333
Mo1	36f	1	0.0979	0.7284	0.0248	1.0000
Mo2	18e	2	0.2874	0.2874	0.2500	0.5000
O1	36f	1	0.1056	0.5876	0.0311	1.0000
O2	36f	1	0.1577	0.6457	0.0035	1.0000
O3	36f	1	0.2008	0.7397	0.0502	1.0000
O4	36f	1	0.1277	0.9267	0.0182	1.0000
O5	36f	1	0.2887	0.4747	0.2467	1.0000
O6	36f	1	0.1647	0.1926	0.2731	1.0000

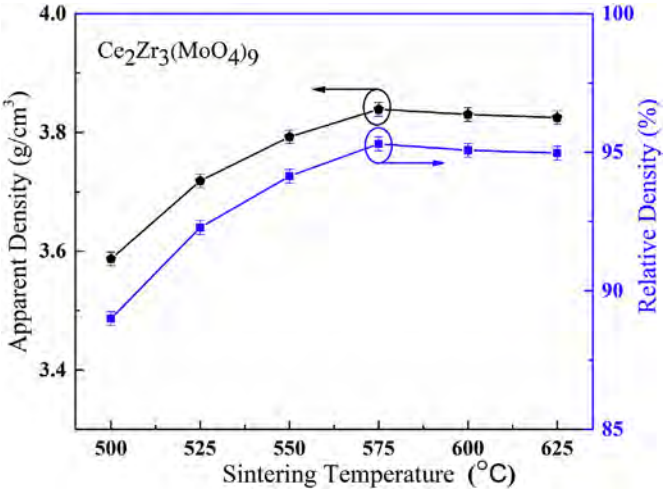

Fig. 5. Apparent and relative density of Ce2Zr3(MoO4)9 ceramics as a function of sintering temperature.

$$\alpha_{obs} = \frac{1}{b} V_m \frac{\varepsilon_r - 1}{\varepsilon_r + 2} \quad (5)$$

where V_m is the molar volume and b is a constant value ($4\pi/3$). The theoretical dielectric polarizability was about 123.93, which was closed to the observed value (149.85), suggesting the accuracy of the theoretical calculation of the dielectric polarizability.

In addition, the quality factor increased from 15,230 GHz at 500 °C to 19,975 GHz at 525 °C, and then kept stable at 525–575 °C. The

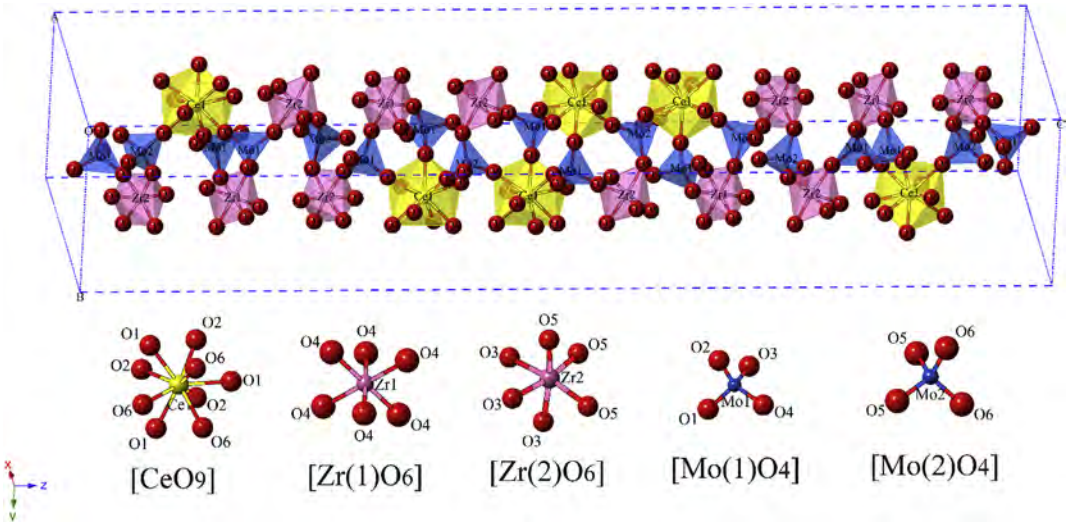

Fig. 4. Schematic diagram of the crystal structure for Ce2Zr3(MoO4)9 ceramics.

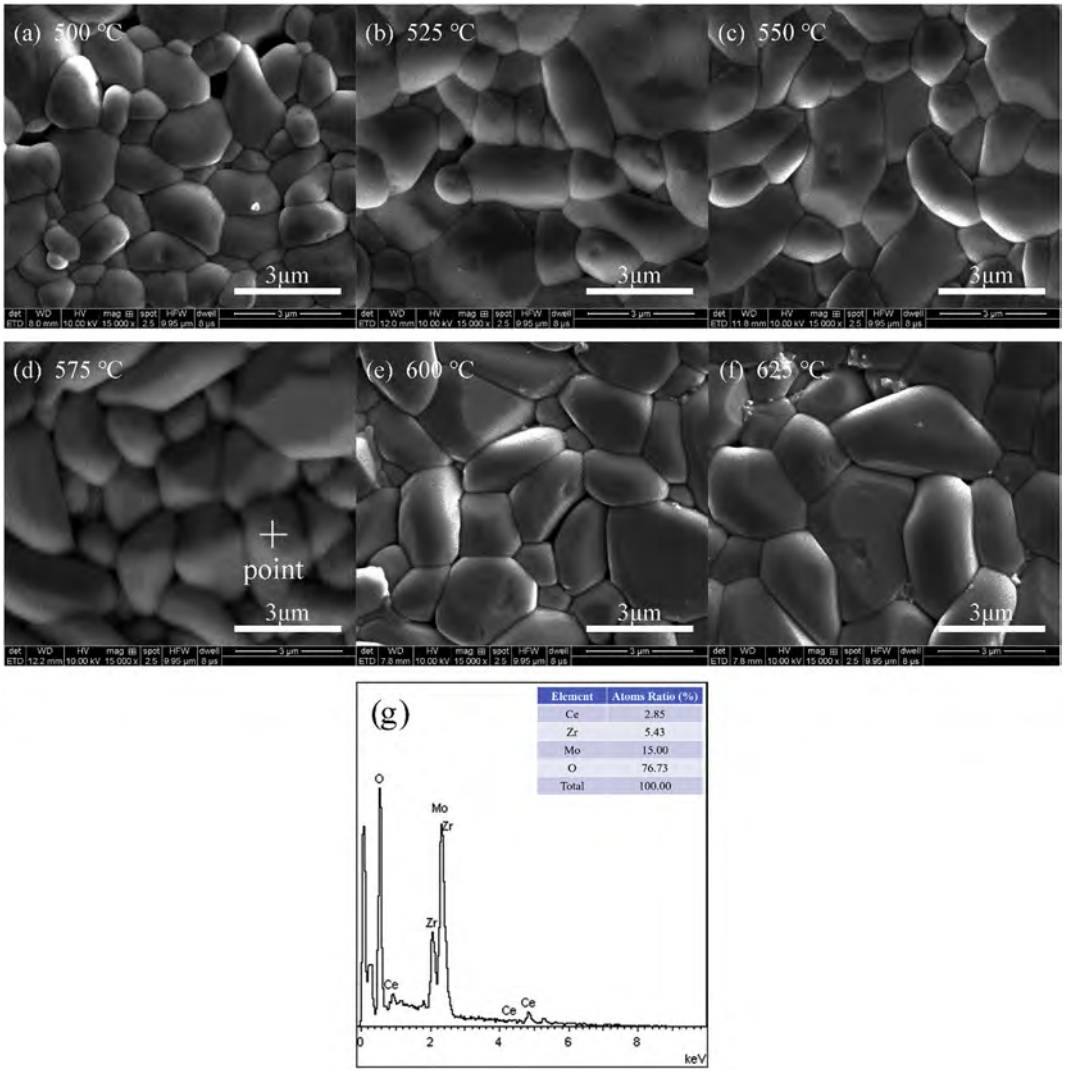

Fig. 6. Typical SEM micrographs of Ce2Zr3(MoO4)9 ceramics fired at (a) 500 °C, (b) 525 °C, (c) 550 °C, (d) 575 °C, (e) 600 °C, (f) 625 °C and (g) EDS analysis about grains selected randomly from the sample sintered at 575 °C.

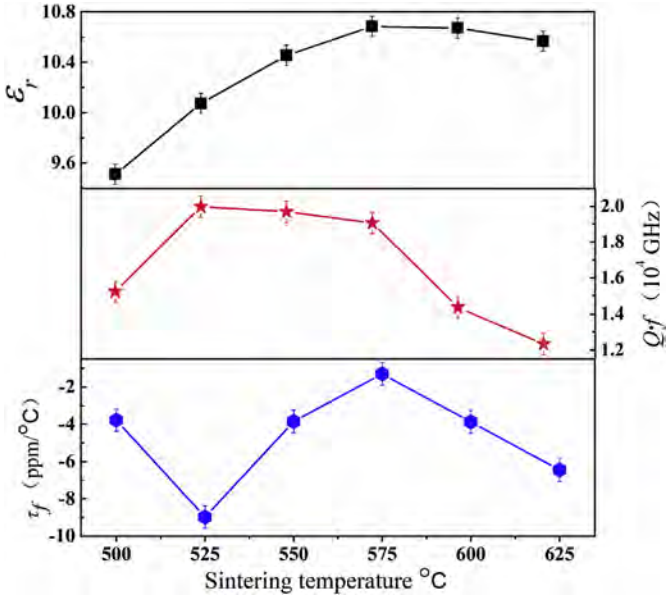

Fig. 7. Curves of εr, Q·f, and τf values of the Ce2Zr3(MoO4)9 ceramics sintered at 500–625 °C.

quality factor declined slightly with further increase of sintering temperature. With an increase in temperature from 500 to 625 °C, the saturation τ_f value of −4.7 ppm/°C was obtained. In general, the microwave dielectric properties are associate with the extrinsic factors, including density, the secondary phase, grain size, impurities, pores, etc., and intrinsic factors, dependent on the structure characteristics [28]. The influences of extrinsic factors on the properties can be neglected when the sintered samples are compact. The relationships between dielectric properties and crystal structure should be investigated. Chemical bonds theory of complex crystals involving bond ionicity f_i, lattice energy U, bond energy E, coefficient of thermal expansion α had been studied to explore the effects of chemical bond on crystal structure. Therefore, the influences of chemical bonds on microwave dielectric properties could be obtained. The sum of binary crystals could be written as shown in Eq. (6) based on the Phillips-Van Vechten-Levine (P–V-L) theory [29–31]. Effective valence of Ce, Zr and Mo were $P_{Ce} = 3$, $P_{Zr} = 4$ and $P_{Mo} = 6$, respectively. The effective valence of O should be followed by the subformula.

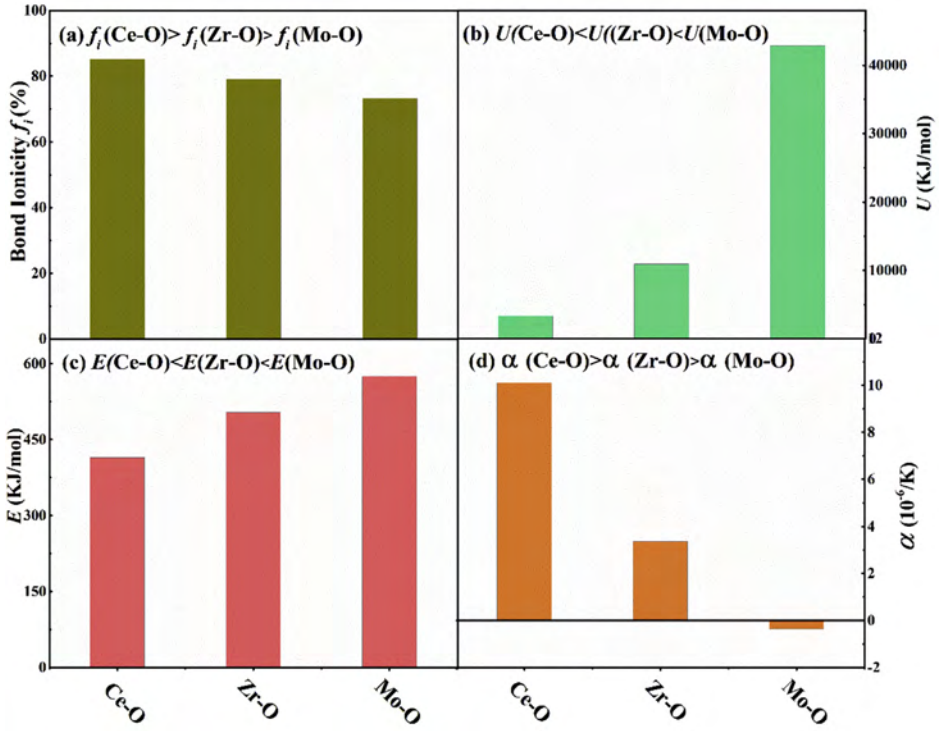

Fig. 8. (a) Bond iconicity, (b) lattice energy, (c) bond energy, and (d) thermal expansion coefficient for Ce2Zr3(MoO4)9 ceramics sintered at 575 °C.

$$\begin{aligned} Ce_2Zr_3(MoO_4)_9 \rightarrow\ & Ce_2 + Zr(1) + Zr(2)_2 + Mo(1)_6 + Mo(2)_3 + O \\ & (1)_6 + O(2)_6 + O(3)_6 + O(4)_6 + O(5)_6 + O(6)_6 \\ \rightarrow\ & Ce_{2/3}O(1)_3 + Ce_{2/3}O(2)_3 + Ce_{2/3} \\ & O(6)_3 + Zr(1)O(4)_3 + Zr(2)O(3)_3 + Zr(2)O \\ & (5)_3 + Mo(1)_{3/2}O(1)_3 + Mo(1)_{3/2} \\ & O(2)_3 + Mo(1)_{3/2}O(3)_3 + Mo(1)_{3/2} \\ & O(4)_3 + Mo(2)_{3/2}O(5)_3 + Mo(2)_{3/2}O(6)_3 \end{aligned} \tag{6}$$

The dielectric constant can be predicted based on the f_i value as shown in Fig. 8(a) [32]. The bond ionicity can be calculated by using Eqs. (7–11) [29–31]:

$$\varepsilon = \frac{n^2 - 1}{1 - f_i} + 1 \tag{7}$$

$$f_i^{\mu} = \frac{(C^{\mu})^2}{(E_g^{\mu})^2} \tag{8}$$

$$(E_g^{\mu})^2 = (E_h^{\mu})^2 + (C^{\mu})^2 \tag{9}$$

$$(E_h^{\mu})^2 = \frac{39.74}{(d^{\mu})^{2.48}} \tag{10}$$

$$C^{\mu} = 14.4 b^{\mu} \exp(-k_s^{\mu} r_0^{\mu})\left[(Z_A^{\mu})^* - \frac{n}{m}(Z_B^{\mu})^*\right]/r_0^{\mu} \tag{11}$$

where E_g^{μ} is the average energy gap, E_h^{μ} is the homopolar part, C^{μ} is the heteropolar part and $\exp(-k_s^{\mu} r_0^{\mu})$ is thomas-Fermi screening factor [33]. The average ionicity of Ce–O, Zr–O and Mo–O bonds were 85.18 %, 79.08 % and 73.24 %, respectively. Therefore, the f_i value of Ce–O bond provided the majority contribution to the ε_r value of CZM sample.

The lattice energy of CZM sample is evaluated by Eq. (12–15) [29–31], which can be decomposed into ionic part U_{bi}^{μ} and covalent part U_{bc}^{μ}:

$$U_{cal} = \sum_{\mu} U_b^{\mu} \tag{12}$$

$$U_b^{\mu} = U_{bc}^{\mu} + U_{bi}^{\mu} \tag{13}$$

$$U_{bc}^{\mu} = 2100 m \frac{(Z_A^{\mu})^{1.64}}{(d^{\mu})^{0.75}} f_C^{\mu} \tag{14}$$

$$U_{bi}^{\mu} = 1270 \frac{(m+n) Z_A^{\mu} Z_B^{\mu}}{d^{\mu}} \left(1 - \frac{0.4}{d^{\mu}}\right) f_i^{\mu} \tag{15}$$

The maximum average lattice energies was 42,856 kJ/mol, which was obtained in Mo–O bond. It could be concluded that Mo–O bond played a predominant role in affecting quality factor of CZM sample.

Moreover, the bond energy measures the strength of chemical bonds, which is calculated based on the following formulas [34–36]:

$$E^{\mu} = t_c E_c^{\mu} + t_i E_i^{\mu} \tag{16}$$

$$E_c^{\mu} = \frac{(r_{cA} + r_{cB})}{d^{\mu}} (E_{A-A} E_{B-B})^{1/2} (KJ/mol) \tag{17}$$

$$E_i^{\mu} = \frac{1389.088}{d^{\mu}} (KJ/mol) \tag{18}$$

$$t_i = \left| \frac{(S_A - S_B)}{6} \right| \tag{19}$$

$$t_c + t_i = 1 \tag{20}$$

where S_A and S_B are the electronegativities of A and B ions; r_{cA} and r_{cB} are the covalent radii; t_i and t_c are ionic and covalent proportional coefficient of an individual bond μ; homonuclear bond energy $E_{A\text{-}A}$ and $E_{B\text{-}B}$ can be consulted in handbook of bond energies [37]. According to Fig. 8(c) and Table 4, the sequence of E (Mo–O) > E (Zr–O) > E (Ce–O) suggested that Mo–O bond provided a major contribution to CZM structure.

The correlation among the temperature coefficient of resonant frequency τ_f, temperature coefficient of the dielectric constant τ_ε and coefficient of thermal expansion α is shown in Eq. (21), in which α is

Table 4
Bond iconicity, bond energy, lattice energy, and thermal expansion coefficient of $Ce_2Zr_3(MoO_4)_9$ ceramic sintered at 575 °C.

Bond type	d (Å)	f_i^μ(%)	f_c^μ(%)	U_{bc} (kJ/mol)	U_{bi} (kJ/mol)	U (kJ/mol)	E_i (kJ/mol)	E_c (kJ/mol)	E (kJ/mol)	α ($10^{-6}K^{-1}$)
Ce–O(1)[1]	2.381(2)	84.61	15.39	681	2753	3434	336.144(3)	583.077(4)	431.625(1)	9.641(7)
Ce–O(1)[2]	2.381(8)	84.61	15.39	681	2753	3434	336.059(6)	582.930(6)	431.516(4)	9.641(7)
Ce–O(1)[3]	2.382(2)	84.61	15.39	681	2753	3434	336.003(2)	582.832(7)	431.443(9)	9.641(7)
Ce–O(2)[1]	2.549(9)	85.54	14.46	608	2634	3242	313.905(2)	544.501(4)	403.069(0)	10.400(3)
Ce–O(2)[2]	2.550(1)	85.54	14.46	608	2634	3242	313.880(6)	544.458(6)	403.037(4)	10.400(3)
Ce–O(2)[3]	2.550(5)	85.54	14.46	608	2634	3242	313.831(3)	544.373(3)	402.974(2)	10.400(3)
Ce–O(6)[1]	2.520(1)	85.39	14.61	620	2655	3275	317.617(1)	550.940(0)	407.835(3)	10.263(6)
Ce–O(6)[2]	2.520(4)	85.39	14.61	620	2655	3275	317.579(3)	550.874(5)	407.786(8)	10.263(6)
Ce–O(6)[3]	2.520(8)	85.39	14.61	620	2654	3274	317.528(9)	550.787(1)	407.722(0)	10.267(7)
Zr(1)–O(4) × 6	2.036(5)	79.04	20.96	2508	8450	10,958	410.771(9)	681.769(7)	506.072(8)	3.344(4)
Zr(2)–O(3)[1]	2.147(9)	79.92	20.08	2309	8204	10,513	389.467(4)	646.410(0)	479.825(5)	3.620(1)
Zr(2)–O(3)[2]	2.148(5)	79.92	20.08	2308	8202	10,510	389.358(6)	646.229(5)	479.691(5)	3.622(0)
Zr(2)–O(3)[3]	2.148(7)	79.93	20.07	2307	8202	10,509	389.322(4)	646.169(3)	479.646(9)	3.622(7)
Zr(2)–O(5)[1]	1.955(3)	78.32	21.68	2674	8632	11,306	427.830(5)	710.082(3)	527.089(1)	3.144(0)
Zr(2)–O(5)[2]	1.955(6)	78.33	21.67	2674	8632	11,306	427.764(9)	709.973(4)	527.008(2)	3.144(0)
Zr(2)–O(5)[3]	1.956(2)	78.33	21.67	2672	8630	11,302	427.633(7)	709.755(6)	526.846(6)	3.146(2)
Mo(1)–O(1)	1.810(6)	73.38	26.62	10,148	32,479	42,627	517.177(0)	766.830(9)	570.436(5)	−0.343(2)
Mo(1)–O(2)	1.750(1)	72.77	27.23	10,645	33,000	43,645	535.055(5)	793.339(8)	590.156(2)	−0.409(1)
Mo(1)–O(3)	1.773(9)	73.02	26.98	10,444	32,795	43,239	527.876(8)	782.695(8)	582.238(2)	−0.383(2)
Mo(1)–O(4)	1.858(8)	73.82	26.18	9784	32,062	41,846	503.766(2)	746.9464	555.644(7)	−0.290(5)
Mo(2)–O(5) × 2	1.842(7)	73.68	26.32	9903	32,202	42,105	508.167(7)	753.472(6)	560.499(4)	−0.308(2)
Mo(2)–O(6) × 2	1.750(4)	72.78	27.22	10,643	32,997	43,640	534.963(8)	793.203(8)	590.055(0)	−0.408(8)
Ce-$O_{avg.}$	2.484(1)	85.18	14.82	-	-	3317	-	-	414.112(2)	10.102(3)
Zr-$O_{avg.}$	2.044(3)	79.08	20.92	-	-	10,933	-	-	503.740(0)	3.363(8)
Mo-$O_{avg.}$	1.797(5)	73.24	26.76	-	-	42,856	-	-	574.838(3)	−0.357(5)

calculated from Eq. (22–25):

$$\tau_f = -(\frac{\tau_\varepsilon}{2} + \alpha) \tag{21}$$

$$\alpha = \sum_\mu F_{mn}^\mu \alpha_{mn}^\mu \tag{22}$$

$$\alpha_{mn}^\mu = -3.1685 + 0.8376\gamma_{mn} \tag{23}$$

$$\gamma_{mn} = \frac{kZ_A^\mu N_{CA}^\mu}{U_b^\mu \Delta_A}\beta_{mn} \tag{24}$$

$$\beta_{mn} = \frac{m(m+n)}{2n} \tag{25}$$

where F_{mn}^μ is the proportion of μ bond, N_{CA}^μ is the coordination number of μ bond for cation, Z_A^μ is the valence states of cation, and k is Boltzmann constant. The average α of Ce–O, Zr–O and Mo–O were 10.10×10^{-6}/K, 3.36×10^{-6}/K and -0.36×10^{-6}/K, respectively. Hence, the main positive effect to temperature coefficients of resonant frequency was the α value of Mo–O bond because of $\alpha_{Mo\text{-}O} < 0$.

Fig. 9(a) presented the IR reflectivity spectrum of CZM sintered at 575 °C. Eq. (26) is used to calculate the complex dielectric permittivity $\varepsilon^*(\omega)$ based on the model of classical harmonic oscillator, and the complex reflectivity R can be obtained as Eq. (27) [38–40]:

$$\varepsilon^*(\omega) = \varepsilon_\infty + \sum_{j=1}^{n} \frac{\omega_{pj}^2}{\omega_{oj}^2 - \omega^2 + j\omega\gamma_j} \tag{26}$$

$$R = \left| \frac{1 - \sqrt{\varepsilon^*(\omega)}}{1 + \sqrt{\varepsilon^*(\omega)}} \right|^2 \tag{27}$$

where ω_{oj}, ω_{pj} and ε_∞ are the the eigen frequency, plasma frequency and dielectric constant, respectively; γ_j is damping factor; n is the number of transverse phonon modes. In addition, the following formula were used to calculate the dielectric loss tangent tan δ:

$$\tan\delta = \frac{\varepsilon''}{\varepsilon'} = \frac{\sum_{j=1}^{n} \Delta\varepsilon_j(\gamma_j\omega)/\omega_{oj}^2}{\varepsilon_\infty + \sum_{j=1}^{n}\Delta\varepsilon_j} \tag{28}$$

The complex permittivity values and fitted IR reflectivity spectra

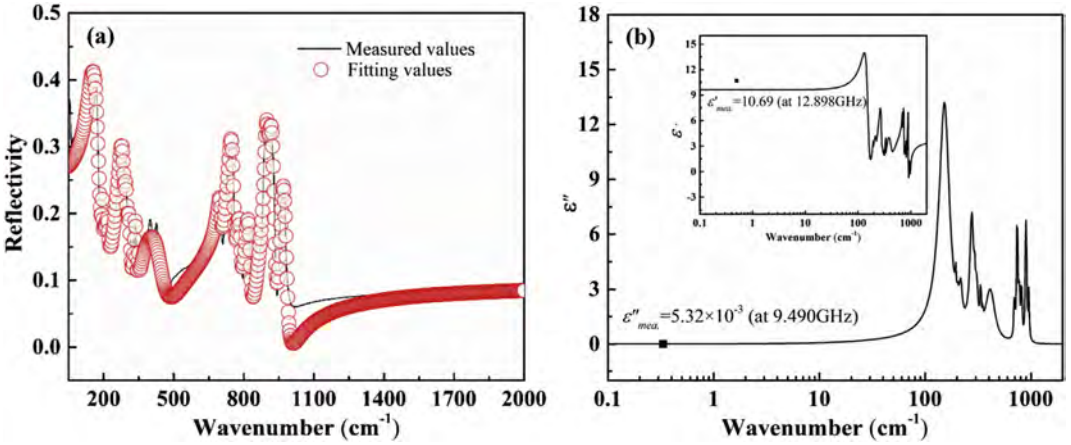

Fig. 9. (a) Measured (black line) and fitted (red line) infrared reflectivity spectrum, and (b) real and imaginary parts of the complex permittivity for Ce2Zr3(MoO4)9 ceramics sintered at 575 °C.

Table 5
Phonon parameters obtained from the fitting of the infrared spectra of $Ce_2Zr_3(MoO_4)_9$ ceramic.

Mode	$Ce_2Zr_3(MoO_4)_9$ ε_∞ = 3.55			
	ω_{oj}	ω_{pj}	γ_j	$\Delta\varepsilon_j$
1	154.01	291.42	42.58	3.58
2	194.74	34.04	4.491	0.03
3	203.99	29.79	7.42	0.02
4	217.64	84.17	17.87	0.15
5	276.80	217.31	27.34	0.62
6	294.71	66.58	9.66	0.05
7	308.27	103.64	18.15	0.11
8	335.93	75.77	7.54	0.05
9	351.08	36.62	4.84	0.01
10	417.08	348.80	103.06	0.70
11	700.34	170.43	16.36	0.06
12	744.83	360.40	24.58	0.23
13	779.66	205.33	21.30	0.07
14	817.31	254.14	25.03	0.10
15	895.36	327.63	17.93	0.13
16	911.61	287.55	26.02	0.10
17	960.27	251.04	24.66	0.07

ω_{oj}, ω_{pj}, γ_j and $\Delta\varepsilon_j$ are the eigen frequency, plasma frequency, coefficient of damping and calculated ε of individual mode, ε_∞ is the dielectric constant affected by electronic polarization in higher frequencies.

were exhibited in Fig. 9(b). There were 17 internal modes based on Table 5. The extra-polated permittivity of CZM was 9.63, which was close to the measured value (10.69). In addition, the calculated dielectric loss of 2.27×10^{-3} was lower than the experimental value of 5.32×10^{-3}, which attributed to various extrinsic loss. Hence, the most polarization contribution for CZM was mainly related to the absorptions of phonon oscillation at infrared region.

4. Conclusion

A new CZM ceramic was fabricated using the solid-state reaction method at a low sintering temperature. A single phase, with trigonal structure in R-3c space group, was confirmed by the X-ray diffractometer. Rietveld refinements were used to further investigate the crystal structure. The dense samples sintered at 575–625 °C with homogeneous microstructures were characterized by Scanning electron microscopy. The structure-property relations of CZM samples were studied by using the chemical bonds theory of complex crystals and far-infrared spectrum. The optimum microwave dielectric properties with ε_r = 10.69, Qf = 19,062 GHz and τ_f = −1.29 ppm/°C were achieved in CZM sample sintered at 575 °C.

Acknowledgments

This work was supported by the National Natural Science Foundation of China (No. 51972143). The authors are thankful to the help of Professor ZhenXing Yue and postdoctoral Jie Zhang on the measurement of microwave properties in Tsinghua University. The authors are also thankful to the administrators in IR beamline workstation of National Synchrotron Radiation Laboratory (NSRL) for the help in IR measurement.

References

[1] L.X. Pang, D. Zhou, Modification of $NdNbO_4$ microwave dielectric ceramic by Bi substitutions, J. Am. Ceram. Soc. 102 (2019) 2278–2282.
[2] X.Q. Song, K. Du, J. Li, R. Muhammad, W.Z. Lu, X.C. Wang, W. Lei, Crystal structures and microwave dielectric properties of novel low permittivity $Ba_{1-x}Sr_xZnSi_3O_8$ ceramics, Mater. Res. Bull. 112 (2019) 178–181.
[3] Y. Wang, T.L. Tang, J.T. Zhang, W.S. Xia, L.W. Shi, Preparation and microwave dielectric properties of new low-loss $NiZrTa_2O_8$ ceramics, J. Alloy. Comp. 778 (2019) 576–578.
[4] Y. Tang, M.Y. Xu, L. Duan, J. Li, J.M. Wu, W.Z. Lu, X.C. Wang, W. Lei, Structure, microwave dielectric properties, and infrared reflectivity spectrum of olivine type Ca_2GeO_4 ceramic, J. Eur. Ceram. 39 (2019) 2354–2359.
[5] W.S. Xia, F.Y. Yang, G.Y. Zhang, K. Han, D.C. Guo, New low-dielectric-loss $NiZrNb_2O_8$ ceramics for microwave application, J. Alloy. Comp. 656 (2016) 470–475.
[6] Y. Wang, S.B. Zhang, T.L. Tang, W.S. Xia, L.W. Shi, Investigation on microwave dielectric properties of new low-loss $CoZrTa_2O_8$ ceramics, Mater. Lett. 231 (2018) 1–4.
[7] H.Y. Yang, S.R. Zhang, H.C. Yang, Y. Yuan, E.Z. Li, Intrinsic dielectric properties of columbite $ZnNb_2O_6$ ceramics studied by P-V-L bond theory and Infrared spectroscopy, J. Am. Ceram. Soc. 102 (2019) 5365–5374.
[8] W.S. Xia, L.Y. Zhang, Y. Wang, S.E. Jin, Y.P. Xu, Z.W. Zuo, L.W. Shi, Extrinsic effects on microwave dielectric properties of high-Q $MgZrTa_2O_8$ ceramics, J. Mater. Sci. Mater. Electron. 27 (2016) 11325–11330.
[9] Y. Wang, L.Y. Zhang, S.B. Zhang, W.S. Xia, L.W. Shi, Sintering behavior and microwave dielectric properties of $MgZrTa_2O_8$ ceramics with fluoride addition, Mater. Lett. 219 (2018) 233–235.
[10] W.S. Xia, L.Y. Zhang, Y. Wang, J.T. Zhang, R.R. Feng, L.W. Shi, Optimized sintering properties and temperature stability of $MgZrTa_2O_8$ ceramics with CuO addition for microwave application, J. Mater. Sci. Mater. Electron. 28 (2017) 18437–18441.
[11] W.S. Xia, F. Jin, M. Wang, X. Wang, G.Y. Zhang, L.W. Shi, Effects of Al_2O_3 additive on sintering behavior and microwave dielectric properties of $ZnTa_2O_6$ ceramics, J. Mater. Sci. Mater. Electron. 27 (2016) 1100–1104.
[12] K. Du, X.Q. Song, J. Li, J.M. Wu, W.Z. Lu, X.C. Wang, W. Lei, Optimised phase compositions and improved microwave dielectric properties based on calcium tin silicates, J. Eur. Ceram. Soc. 39 (2019) 340–345.
[13] W.J. Guo, J. Zhang, Y. Luo, Z.X. Yue, L.T. Li, Microwave dielectric properties and thermally stimulated depolarization of Al-doped $Ba_4(Sm, Nd)_{9.33}Ti_{18}O_{54}$ ceramics, J. Am. Ceram. Soc. 102 (2019) 5494–5502.
[14] X.K. Lan, J. Li, Z.Y. Zou, M.Q. Xie, G.F. Fan, W.Z. Lu, W. Lei, Improved sinterability and microwave dielectric properties of $[Zn_{0.5}Ti_{0.5}]^{3+}$-doped $ZnAl_2O_4$ spinel solid solution, J. Am. Ceram. Soc. 102 (2019) 5952–5957.
[15] X.Q. Song, M.Q. Xie, K. Du, W.Z. Lu, W. Lei, Synthesis, crystal structure and microwave dielectric properties of self-temperature stable $Ba_{1-x}Sr_xCuSi_2O_6$ ceramics for millimeter-wave communication, J Materiomics. https://doi.org/10.1016/j.jmat.2019.07.005.
[16] D. Zhou, L.X. Pang, D.W. Wang, I.M. Reaney, Novel water-assisting low firing MoO_3 microwave dielectric ceramics, J. Eur. Ceram. Soc. 39 (2019) 2374–2378.
[17] S.Z. Hao, D. Zhou, L.X. Pang, The spectra analysis and microwave dielectric properties of $[Ca_{0.55}(Sm_{1-x}Bi_x)_{0.3}]MoO_4$ ceramics, J. Am. Ceram. Soc. 102 (2019) 3103–3109.
[18] H.H. Guo, D. Zhou, L.X. Pang, Z.M. Qi, Microwave dielectric properties of low firing temperature stable scheelite structured (Ca, Bi)(Mo, V)O_4 solid solution ceramics for LTCC applications, J. Eur. Ceram. Soc. 39 (2019) 2365–2373.
[19] W.Q. Liu, R.Z. Zuo, Low temperature fired $Ln_2Zr_3(MoO_4)_9$ (Ln = Sm, Nd) microwave dielectric ceramics, Ceram. Int. 43 (2017) 17229–17232.
[20] W.Q. Liu, R.Z. Zuo, A novel low-temperature firable $La_2Zr_3(MoO_4)_9$ microwave dielectric ceramic, J. Eur. Ceram. Soc. 38 (2018) 339–342.
[21] Y.H. Zhang, H.T. Wu, Crystal structure and microwave dielectric properties of $La_2(Zr_{1-x}Ti_x)_3(MoO_4)_9$ ($0 \le x \le 0.1$) ceramics, J. Am. Ceram. Soc. 102 (2019) 4092–4102.
[22] Y.H. Zhang, J.J. Sun, N. Dai, Z.C. Wu, H.T. Wu, C.H. Yang, Crystal structure, infrared spectra and microwave dielectric properties of novel extra low-temperature fired $Eu_2Zr_3(MoO_4)_9$ ceramics, J. Eur. Ceram. Soc. 39 (2019) 1127–1131.
[23] J. Rodriguez-Carvajal, Recent advances in magnetic structure determination by neutron powder diffraction, J. Phys. Condens. Matter 192 (1993) 55–69.
[24] B.W. Hakki, P.D. Coleman, A dielectric resonator method of Measuring Inductive capacities in the millimeter range, IRE Trans. Microw. Theory Tech. 8 (1960) 402–410.
[25] W.E. Courtney, Analysis and evaluation of a method of measuring the complex permittivity and permeability microwave insulators, IEEE Trans. Microw. Theory Tech. 18 (1970) 476–485.
[26] R.D. Shannon, Dielectric polarizabilities of ions in oxides and fluorides, J. Appl. Phys. 73 (1993) 348–366.
[27] G.K. Choi, J.R. Kim, S.H. Yoon, K.S. Hong, Microwave dielectric properties of scheelite (A = Ca, Sr, Ba) and wolframite (A = Mg, Zn, Mn) $AMoO_4$ compounds, J. Eur. Ceram. Soc. 27 (2007) 3063–3067.
[28] H.Y. Yang, S.R. Zhang, Y.W. Chen, H.C. Yang, Y. Yuan, E.Z. Li, Crystal chemistry, Raman spectra, and bond characteristics of trirutile-type $Co_{0.5}Ti_{0.5}TaO_4$ microwave dielectric ceramics, Inorg. Chem. 58 (2019) 968–976.
[29] D.F. Xue, S.Y. Zhang, Calculation of the nonlinear optical coefficient of the $NdAl_3(BO_3)_4$ crystal, J. Phys. Condens. Matter 8 (1996) 1949–1956.
[30] Z.J. Wu, Q.B. Meng, S.Y. Zhang, Semi empirical study on the valences of Cu and bond covalency in $Y_{1-x}Ca_xBa_2Cu_3O_{6+y}$, Phys. Rev. B 58 (1998) 958–962.
[31] Q.B. Meng, Z.J. Wu, S.Y. Zhang, Evaluation of the energy barrier distribution in many-particle systems using the path integral approach, J. Phys. Condens. Matter 10 (1998) 85–88.
[32] S.S. Batsanov, Dielectric methods of studying the chemical bond and the concept of electronegativity, Russ. Chem. Rev. 51 (1982) 684–697.
[33] B.F. Levine, Bond susceptibilities and ionicities in complex crystal structures, J. Chem. Phys. 59 (1973) 1463–1486.
[34] R.T. Sanderson, Multiple and single bond energies in inorganic molecules, Inorg. Nucl. Chem. Lett. 30 (1968) 375–393.
[35] R.T. Sanderson, Chemical Bonds, Bond Energy, Academic press, New York, 1971.
[36] R.T. Sanderson, Electronegativity and bond energy, J. Am. Chem. Soc. 105 (1983)

2259–2261.
[37] Y.R. Luo, Comprehensive Handbook of Chemical Bond Energies, CRC press, Boca Raton, 2007.
[38] J. Petzelt, S. Kamba, Submillimetre and infrared response of microwave materials: extrapolation to microwave properties, Mater. Chem. Phys. 79 (2003) 175–180.
[39] K. Wakino, M. Murata, H. Tamura, Far infrared reflection spectra of Ba(Zn, Ta)O_3-$BaZrO_3$ dielectric resonator material, J. Am. Ceram. Soc. 69 (1986) 34–37.
[40] W.B. Li, D. Zhou, H.H. Xi, L.X. Pang, X. Yao, Structure, infrared reflectivity and microwave dielectric properties of $(Na_{0.5}La_{0.5})MoO_4$-$(Na_{0.5}Bi_{0.5})MoO_4$ ceramics, J. Am. Ceram. Soc. 99 (2016) 2083–2088.